Evaluation of the impact performance and energy absorption capabilities of 3D printed Composites

Russo Swart, Feras Korkees, Peter Dorrington, and Joshua Thurman
Faculty of Science and Engineering, Swansea University, Swansea, UK

Abstract

Purpose - Composites 3D printing has the potential to replace the conventional manufacturing processes for engineering applications since it allows for the manufacturing of complex shapes with the possibility of reducing the manufacturing cost. The current paper analyses the performance of 3D printed fibre reinforced polymer composites to investigate the energy absorption capabilities and the residual properties before and after impact.
Methodology -Various composites comprised of carbon fibres (CF) and Kevlar fibres embedded into both Onyx and nylon matrix was printed using Markforged-Two 3D printers. Specimens with different fibre orientations and fibre volume fractions (V_f) were printed. A Drop-weight impact test was performed at energies of 2J, 5J, 8J and 10J. Flexural testing was performed to evaluate the flexural strength, flexural modulus, and absorbed energy under bending (AEUB) before and after impact. Additionally, 3D printed carbon fibre composites were tested at two different temperatures to study their behavior under room and sub-ambient temperatures. Failure modes were investigated using optical and high depth of field microscopes for all 3D printed composite samples.
Findings - Kevlar/nylon composites with a unidirectional (UD) lay-up, and 50 % volume fraction (V_f) exhibited the most prominent results for AEUB at room temperature. The high-volume fraction carbon fibre composite showed the highest ultimate strength, and modulus and performed best at both temperature regimes.
Originality - The work, findings and testing produced in the current paper are entirely original with the objective to provide further understanding of 3D printed composites and its potential for use in many applications.

Keywords – Composites, 3D printing, Fibres, impact resistance, mechanical properties, nylon, Onyx

1. Introduction

Fibre-reinforced polymer composites (FRPC) have had a significant contribution and impact in various engineering applications such as the automotive, aircraft, and mass transport industries to name a few. The combination of plastic and fibres produces lightweight, strong, and durable materials which are crucial factors for applications which demand weight saving, cost saving, and importantly impact strength as top priorities (Njuguna, 2016). The increase in usage and popularity of composites are due to the outstanding properties of these materials including lightweight, high strength, good fracture

resistance, and a high damage tolerance. When polymer materials are combined with fibres it can reduce the overall weight of a specific entity by 20%-40%. Commonly this is seen in modern military aircrafts, where there is a weight reduction factor of 30%, along with an increase in damage tolerance. It goes without notice, that the use of composite-based components replace metal in terms of part maintenance cycles, and their use is growing rapidly in commercial and leisure aviation (Mouritz, 2012).

3D printing technology of fibre reinforced polymer composites is a relatively new and advanced manufacturing technology that is continuing to grow. It is a very effective way of designing and creating composites (Taormina *et al.,* 2018). The rapid prototyping of the 3D products and utilization of computer-aided design (CAD) gives the freedom to switch between different design parameters to generate an intricate and geometrically accurate bespoke design, such as custom head supports in wheelchairs (Howard *et al.,* 2020). The 3D printing industry is growing fast through applications in biomedical engineering, general engineering, and sports science (Sadasivuni, Deshmukh and Al-Maadeed, 2020). Polymer composites and epoxy laminates are commonly manufactured through conventional techniques i.e., hand lay-up or flexible vacuum tooling. Other common conventional processes consist of wet lay-up, vacuum bagging, resin transfer moulding, pultrusion, and automated lay-ups. Consequently, these processes are very labor intensive (wet lay-up, vacuum bagging) and significantly expensive (automated lay-ups) (Agarwal *et al.,* 2018). These techniques often require expensive production tooling which due to the need to reduce undercuts, or include cores in tooling, can constrain the geometry of the part that is designed (Fink, 2018). These geometric limitations can be overcome-albeit on a smaller scale with fibre-reinforced 3D printing.

3D printing allows for complex internal structures and low wastage, making its benefits outweigh that of conventional methods when dependent on complexity, shape, and novel design, particularly that of composite filament fabrication (CFF). CFF results in a part with enhanced mechanical properties in contrast to the familiar fused deposition modelling (FDM) or fused filament fabrication (FFF) techniques (Agarwal *et al.,* 2018). It removes any necessity for molds or autoclaves compared to conventional techniques, allowing for a selection of polymers and positioning of fibre layers. The CFF approach outweighs majority of the drawbacks seen in FFF and FDM 3D printing (Agarwal *et al.,* 2018). Despite the popular usage of 3D printed FRPCs in the mentioned sectors, impact resistance is still of some concern. This is because fabricated composite parts, can experience impacts while in service (e.g., foreign object impact and environmental exposure). Damage to composite structures subjected to different impact scenarios is therefore an important study in current research studies (Hosseinzadeh, Mehrdad Shokrieh and Lessard, 2005).

Impact damage is significantly detrimental to a composite structure because propagation of microcracks and the occurrence of delamination could arise (Flansburg, Engelstad and Rousseau, 2010). However, the most relevant cause for delamination in composites is the low velocity impacts which can further result in fibre breakage and microscopic damage which could go unnoticed (Žmindák and Dudinský, 2012). These factors are especially destructive to the composite structure as further damage can occur such as matrix cracking, inter-laminar damage, and debonding between fibres and the matrix (Korkees, Arnold and Alston, 2018). Damage modes experienced by the composite structure can then influence the amount of energy it is capable of absorbing. If composites structures are further utilized in service in its damaged state catastrophic failure could occur (Caminero *et al.,* 2018). During impact three modes of energy absorption could occur, fibre and matrix debonding, delamination, and fiber breakage as mentioned previously. These failure modes result in a reduction of load carrying abilities for the composite structure as a whole (Zhang *et al.,* 2013)(Olsson, 2012). This was similarly seen in the work of

(S. M.Fijul Kabir, Mathur and Seyam, 2020a) displaying crack initiation sites with localized compressive loads. Propagation took place on the neutral axis resulting in fibre breakage failing under a bending load. Additionally, studies indicated that if crack initiation sites were minimized, an increase in toughness can be seen (Swolfs and Pinho, 2016). Therefore this poses significant importance to consider energy absorption capabilities and the damage induced from low-velocity impact in a composite system.

There has been several studies showing the fundamental influence on the mechanical properties and the failure modes of composite structures. Exhibited in the work of (Korkees, Arnold and Alston, 2018), low velocity impact tests were performed to evaluate the flexural characteristics and failure modes of ±45° carbon/epoxy laminates. Investigation was done under various conditions, and they were inspected before and after being subjected to these conditions. A conclusion was made that impacting under low velocity did cause deformation to the structures and led to fractures of the fibres and thus a reduction of load carrying abilities (Korkees, Arnold and Alston, 2018). A research study carried out by (AlOmari *et al.,* 2020) showed that the amount of energy absorbed related to the thickness of a single layer, number of layers, and stacking sequence. It was concluded that the stacking sequence of [90/0/45/-45]s was better than [60/45/-45/-60]s showing great importance and reliance on stacking sequence (AlOmari *et al.,* 2020). Further research was conducted by (Korkees et al. 2020) (Korkees, Allenby and Dorrington, 2020) on 3D printed carbon fibre/nylon composites and found that by increasing the fibre volume fraction, the flexural strength and the stiffness of 3D printed composites increased. (Cazón-Martín *et al.,* 2019) used the process of 3D printing and employed it to create a novel design of shin pads for football players. This allowed for twenty-four different geometries to be evaluated using a 1-kg impactor released from several heights. It was finalized that the additive manufactured specimens tested at the highest drop height had a lower impact acceleration than the commercial shin pads, as well as an improvement in penetration resistance from 13% to 32% for the additive manufactured samples.

In regards to fibre placement, lay-ups, and orientations (Kabir, Mathur and Seyam, 2021) attempted to maximize the performance of 3D printed (3DP) FRPCs. They 3D printed fibreglass-reinforced nylon composites with the highest amount of fibre content possible by the 3D printer, with varying fibre orientations (0/0°,0/90°, ±45° and 0/45/90/-45°) was manufactured. Each number refers to an individual fibre orientation separated by a '/' which indicates the next layer of fibre and its orientation. Tensile testing and drop-weight testing were performed to investigate their performance properties. The results showed that the samples with the highest amount of fibre content had a favorable effect on their performance by improving its properties. Additionally, the 3DP samples were compared to a traditional orthogonal woven composite and showed that the 3DP samples displayed delamination due to poor matrix infusion and insufficient through-thickness reinforcement. However, there was exceptional increase in the impact strength by 224% (Kabir, Mathur and Seyam, 2021). Impact testing on 3D printed composite samples using a Mark Two printer was reviewed by (S. M.Fijul Kabir, Mathur and Seyam, 2020b) showing numerous studies on impact testing methods. The impact resistance was evaluated by investigating failure mechanisms to assess their suitability for prospective high-performance applications. Substantial performance of the 3D printed specimens with various fibre orientations was noticed in comparison to 3D orthogonal plain-woven composites. (Caminero *et al.,* 2018) studied damage imposed from impact to 3D printed continuous fibres using CFF technology (Markforged Mark Two). They utilized a nylon matrix and the use of carbon, glass, and Kevlar fibres as reinforcement. Two types of fibre patterns were selected, i.e, concentric and isotropic, where the isotropic pattern provided better properties. The samples flexural properties were analyzsed subjected to a three-point bending test.

Conclusions showed that the impact strength increased as the fibre volume content increased across all samples with fibre inclusion.

(Dickson *et al.,* 2017) evaluating the performance of continuous carbon, Kevlar and glass fiber reinforcement with the older generation Markforged Mark One. The flexural properties of these samples were investigated, alongside the influence of fibre orientation, fibre type and volume fraction. Samples with carbon fibres provided the highest mechanical strengths and a 5-fold enhancement was seen in their flexural strengths across all fibre reinforced samples. CFF characterization was implemented, and layers of continuous carbon fibres were embedded into a polymers matrix (PA6) using statistical methods and mechanical examination(Araya-Calvo *et al.,* 2018). This was done to evaluate the reinforcement pattern, distribution of fibres, and volume fraction. Samples were printed with the Markforged Mark Two printers and improvement in flexural response was noticed with a concentric fill pattern, using 0.4893 carbon fibre volume ratio, perpendicular to the applied force. Synergistic reinforcement of short fibres and continuous fibres within a nylon matrix was studied (Peng *et al.,* 2019). It was concluded that the tensile strength for both continuous and short fibres was more superior to that of individual carbon fibre reinforcement. In addition, it was clear that short carbon fibres showed higher mechanical properties due to stronger adhesion of the interfaces in contrast to continuous CFs.

Additionally other studies were conducted reviewing fibere volume fraction and the influence of fibres in composites (Omar et al., 2019), and impact tests were performed by (Luo *et al.,* 2019) and (Caminero *et al.,* 2018). A general review of flexural performance ((Goh *et al.,* 2017), impact performance, statistical analysis of material properties (Araya-Calvo *et al.,* 2018), FEA/simulations (Swolfs and Pinho, 2016), and mechanical analysis was done on 3D printed continuous fibre-reinforced composites conducted by (S. M.Fijul Kabir, Mathur and Seyam, 2020a). ..

In this study, the impact and flexural behaviors of various 3D printed FRPC, were investigated. Mark Forged Mark Two Desktop printers were used to print the composite samples. These are commercially available desk based FRPC 3D printers. The materials used in the composite samples are Kevlar and carbon fibres (CF) as reinforcement and nylon and Onyx as matrix materials. Different fibre volume fractions, fibre layer locations, and fibre orientations were considered. Printed samples were first impacted at low energies and different temperatures followed by a three-point bending test. This was to evaluate the energy absorption capabilities and residual properties of the printed samples before and after impact. The failure modes of the composites were also investigated using optical microscopes.

2. Experimental work

The polymer materials used for fabrication were 800cc Nylon white filament, which is a non-abrasive engineering thermoplastic, chosen mainly for its high impact resistance, toughness, and versatility. Additionally, 800 cc Onyx filament was used for the testing of sub-ambient samples and room temperature samples. It offers high strength, excellent heat resistance and a high surface finish. It functions as a thermoplastic matrix. All specimens flexural tested and impacted had dimensions of 80 x 15 x 3 mm and were designed using SolidWorks 2019. The slicing software used to “slice” these test parts into the required .gcode and enable parameter variations was that of Eiger. Batches of samples were fabricated with different lay-ups including isotropic unidirectional (UD), Quasi-isotropic (QI) [0/45/90/135°], concentric unidirectional (Figure 1), and short fibres (Onyx). Three samples were printed for each continuous fibre orientation, short fibres, and for those with no fibres embedded (nylon samples). This was done to calculate an average result for each group. The batch of samples were specified as follows; 36 CF concentric samples

impacted at room temperature (RT) (Table 2), and 36 CF concentric samples impacted at low temperature (LT)(Table 3). Additionally, 36 Kevlar/nylon samples were fabricated, and 36 fabricated CF/nylon samples, with the lay-ups of QI and UD. In total 144 samples were manufactured, utilizing the Mark Forged Mark Two Desktop series 3D printer. All printing parameters are tabulated in Table 1, these specifications were set as recommended by the Eiger software for optimum print quality, time of prints and to ensure there is no waste of plastic material. Only changes to the fibre layers, orientation of fibres and fill type was made. Orientation was set to 0° for X, Y and Z. Printed samples with high fibre volume fraction (50% V_f.) have 22 fibre layers for the Kevlar reinforcement and 16 fibre layers for the CF reinforcement. This is since CF fibres have a larger diameter. However, no triangular fill density was set, as maximum fill density was reached for these samples. On the contrary, the low volume fraction (20% V_f.) samples have 8 fibre layers with a triangular fill density, for both fibre types. The batch tested at LT and RT was fabricated to test UD CF reinforcement with a concentric pattern, short fibres (Onyx), and nylon with no fibre reinforcement. The number of rings for concentric samples was set to 6. This was the maximum number of rings possible to fit within the width of the samples (w=15mm). Impact testing was done on unreinforced and reinforced specimens at LT and RT. Low temperature was achieved by submerging the samples in liquid nitrogen at -196°c for 2 hours before impact. Both nylon and Onyx filament were immediately placed in a sealed dry box, Pelican 1430 case, preventing moisture absorption upon unpackaging of the plastic; therefore, no drying of the material was necessary. Tables 2 and 3 show the various lay-ups with their Vf% used for the composites and the energies impacted. A drop-weight impact test was firstly carried out on all samples and generated the required impact energy at different heights and weights of the impactor, Table 4. The following equation was used to calculate the impact energies.

$$\text{Potential Energy (PE)} = \text{mass (Kg)} \times \text{gravity (9.8 m/s2)} \times \text{height (m)} \quad (1)$$

The volume of fibre (Fv) and plastic (Pv) for each sample was estimated by Eiger software in (cm^3) and was used to determine the fibre volume fraction (V_f) of the sample. Eiger calculates these parameters by its own algorithm to determine the values for Fv and Pv. This is based off of the quantity of fibre layers used and the quantity of plastic to create a sample. These values can be extrapolated and inputted into Equation 2 to calculate the V_f.% of the printed samples. However, the calculation of V_f.% is not an exact representation because all fibre reinforcement (Kevlar and CF) consists of a nylon sizer to enable the laying up of fibres upon extrusion into the matrix (Korkees, Allenby and Dorrington, 2020)(S M Fijul Kabir, Mathur and Seyam, 2020). However, it provides some relative accuracy, enough to accurately distinguish between mechanical properties. The values Fv and Pv calculated by Eiger and inputted into Equation 2 produced a value for Vf. The same method was applied for samples consisting of short fibres as Eiger calculates it with the same methodology as continuous fibres. Plastic and fibre specifications of all samples was tabulated in Table 5.

$$V_f = [\text{fibre volume} / [(\text{fibre volume} + \text{plastic volume})] \times 100) \quad (2)$$

Flexural tests were performed using a Hounsfield H25KS machine with a 25kN load cell at a test speed (u) of 2 mm/min recording every 0.2 seconds. Samples were all tested until complete failure and all flexural properties were calculated using the British standard BS EN ISO 14125:1998+A1:2011 (British Standards Institution, 2011). The absorbed energy under bending was determined by calculating the area under the created stress-strain graphs. Furthermore, an optical microscope (Zeiss SmartZoom digital microscope) and Keyence VHX-1000 was used to examine all specimen microstructures and the failure modes after impact

and flexural testing. Impact testing of samples were based on the standard ASTM D7136/D7136M-12 (ASTM International, 2012).

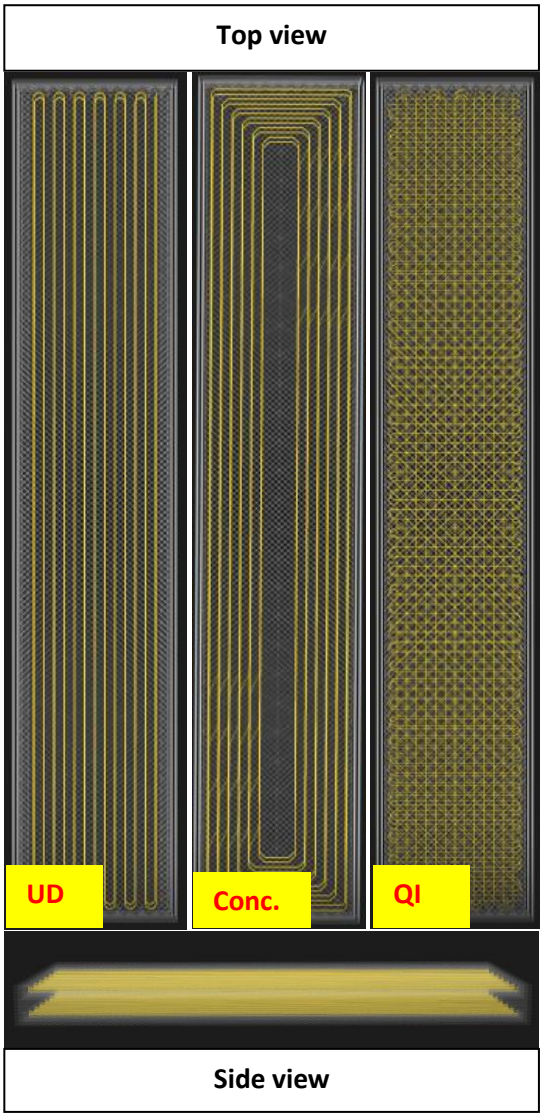

Figure 1 Slicer software Eiger, lay-ups and fibre orientations

Table 1 Printing parameters

Printing parameters	
Material (Plastic)	Nylon- End of Life/Onyx
Reinforcement material	Kevlar/CF
Layer Height	0.1 (mm)
Use of supports	No supports
Fill pattern	Triangular fill
Fill density	50%
Roof & floor layers	4
Wall layers	2
Total fiber layers (Isotropic)	8/16/22
Concentric fiber rings	6

Table 2 Passed and failed subjects at room temperature

Impact at Room Temperature				
Material	**0J**	**2J**	**5J**	**8J**
Onyx	Pass	Fail	Fail	Fail
Nylon	Pass	Pass	Fail	Fail
CF/nylon (20% *Vf*)	Pass	Pass	Pass	Fail
CF/nylon (50% *Vf*)	Pass	Pass	Pass	Pass

Table III Passed and failed subjects at low temperature

Impact at Low Temperature				
Material	**0J**	**2J**	**5J**	**8J**
Onyx	Pass	Fail	Fail	Fail
Nylon	Pass	Fail	Fail	Fail
CF/nylon (20% *Vf*)	Pass	Pass	Fail	Fail
CF/nylon (50% *Vf*)	Pass	Pass	Pass	Fail

3. Results and Discussion

3.1. Microstructure inspection

Following the fabrication of the composite samples, the quality of the samples in terms of the bonding between fibre layers, the fibre distribution, and fibre orientations was inspected using optical microscopy. It can be seen from both Figures 2 and 3 that the printed samples are of a good quality. The bonding between the layers is strong and there is no indication of delamination between them or actual delamination. The UD Kevlar (Figure 2a. and 2c.) and CF (Figure 3b. and 3d.) specimens have fibres all going in the longitudinal direction but with different total number of fibre layers in comparison to one another (16 layers for CF and 22 layers for Kevlar). This was apparent in Figure 2a. and 2c. and Figure 3b. and 3d. where it was visible that Kevlar fibres had a higher packing arrangement. This is because Kevlar fibres are smaller than CF fibres in diameter (Kevlar=0.33mm, and CF=0.39mm), allowing more fibres to be combined into the matrix within the same thickness of the samples. Figure 2d. and Figure 3c. exemplify QI samples where the directions (0/45/90/135°) are seen clearly. It can be assertively noticed that all printed composite samples have good structural quality.

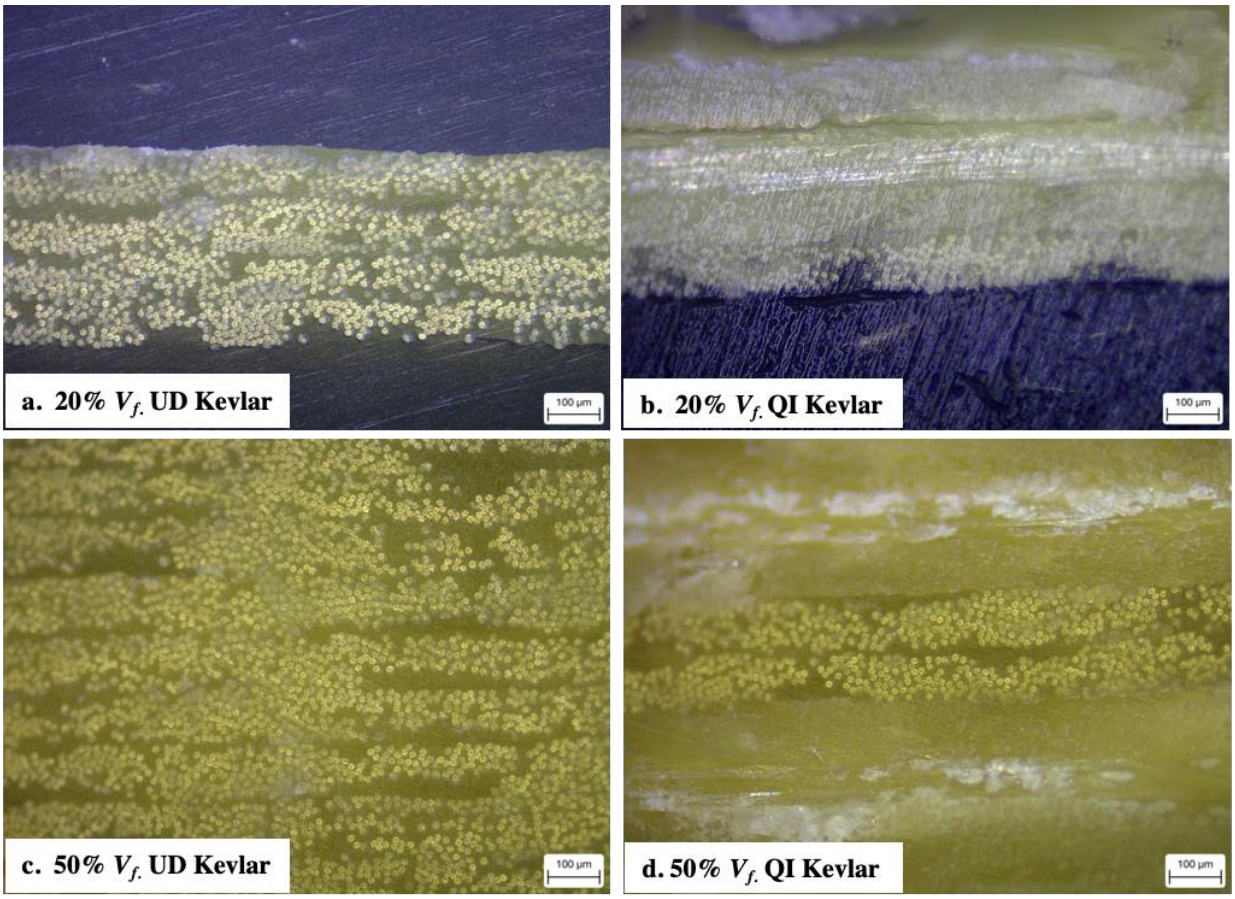

Figure 2 Micrographs of 3D printed Kevlar samples

Table 4 Calculated impact energies

Energy (J)	Weight (N)	Height (M)
2	5	0.25
5	5	0.61
10	5	1.22
10	10	0.75

Table 5 Plastic and fibre specifications

Plastic and fiber specifications				
Material	**Pv (cm^3)**	**Fv (cm^3)**	**V_f (%)**	**Weight (g)**
Nylon	2.47	N/a	N/a	2.71
Onyx	2.5	N/a	N/a	2.95
HVF Kevlar isotropic (UD)	1.65	1.95	54.16	4.26
LVF Kevlar isotropic (UD)	2.42	0.71	22.68	3.55
HVF CF isotropic (UD)	1.83	1.71	48.31	4.4
LVF CF isotropic (UD)	2.51	0.85	25.3	3.96
HVF CF (concentric)	1.72	1.93	52.87	4.86
LVF CF (concentric)	2.77	0.86	23.69	4.16
HVF CF (90°)	1.57	1.71	52.13	4.12
LVF CF (90°)	2.39	0.85	26.23	3.82
HVF Kevlar (90°)	1.63	1.96	54.60	3.98
LVF Kevlar (90°)	2.56	0.71	21.71	3.45
HVF CF (QI)	1.90	1.71	47.37	4.24
LVF CF (QI)	2.66	0.86	24.43	3.88
HVF Kevlar (QI)	1.73	1.96	53.12	4.09
LVF Kevlar (QI)	2.59	0.71	21.51	3.49

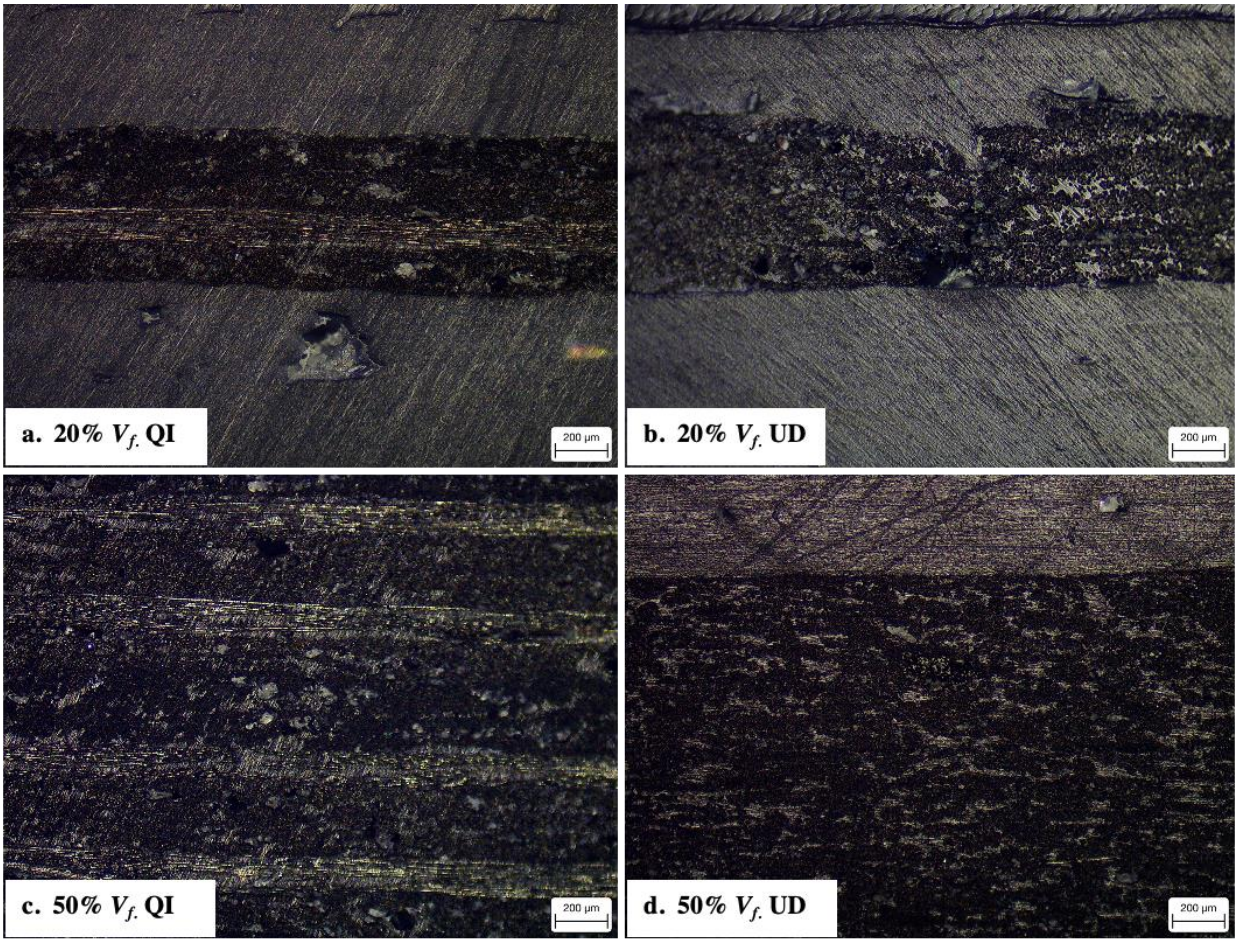

Figure 3 Micrographs of 3D printed Carbon fibre samples

3.2 Impact performance

Tables 2, 3, and 4 present a matrix of all tested samples, where passed and failed indicated which samples reached ultimate failure. This was determined when the matrix and fibres were separated resulting in no further tests that could be done, similarly seen in Figure 4d. The impact energies considered in this study are given in table 4. Figure 4 show the failure modes witnessed after impacting the samples, and in Figure 4b. it shows the highest impact energy tested and the succession of the sample due to the UD layup. Only slight debonding of fibres and apparent delamination had occurred to the Kevlar sample in Figure 4b. The drop-weight impactor used is represented in Figure 5.

Up to this point, it was noticed that there were different behaviors when the samples reacted to an applied load. To elaborate, Tables 6 and 7 displays statistical analysis of the CF/nylon and Kevlar/nylon samples, respectively, with their averaged flexural and energy values tabulated. In comparison to CF samples, it indicated that Kevlar/nylon composites had values further below from the mean value as indicated by the standard deviation (σ) values. Tables 8-10 present a matrix of passed and failed subjects (Table 10), in addition with their properties obtained after impacting and flexural testing (Tables 8 and 9). It was noted that Kevlar samples experienced greater impact energy yet displayed fewer signs of damage

(Figure 4a. and b.) compared to CF samples, also seen in Table 8. On the contrary, the CF sample in Figure 4d. had a visible brittle failure, due to the sudden failure and rapid crack propagation. Contradicting this, Kevlar samples in Figure 4, reacted with a ductile behavior due to the large deformation before definite failure, seen as signs of bending and indentation to the samples. Kevlar experiences a common failure mode known as Euler buckling of individual fibres as well as kinking band formations which was distinguished in Figure 4a. This is interpreted by the split ends of fibres forming fine fibrils. This occurs due to the structural instability of individual fibres under axial load and the anisotropic nature of Kevlar fibre's microstructure (Hull and Clyne, 1996).

To note, tests were not further proceeded for virgin material (nylon on its own) as failure commenced at 2J in Tables 2 and 3, and Figure 4e. Failure occurred to nylon because the matrix had to cope with a greater quantity of the load subject to no fibre reinforcement. This results in inadequate enhancement of strength. Therefore, less stiffness and strength, and hence failure (Chawla, 1998b, 1998a).

3.3. Flexural performance before and after impact

It is necessary to analyze the flexural performance of composites as they commonly experience in-service impact defects, and these defects would determine their service life, similarly studied by (Flansburg, Engelstad and Rousseau, 2010). Therefore, the flexural modulus, flexural strength, and energy absorbed were determined before and after impact, in figure 6, and their values obtained are shown in Figures 7,8 and 9, respectively.

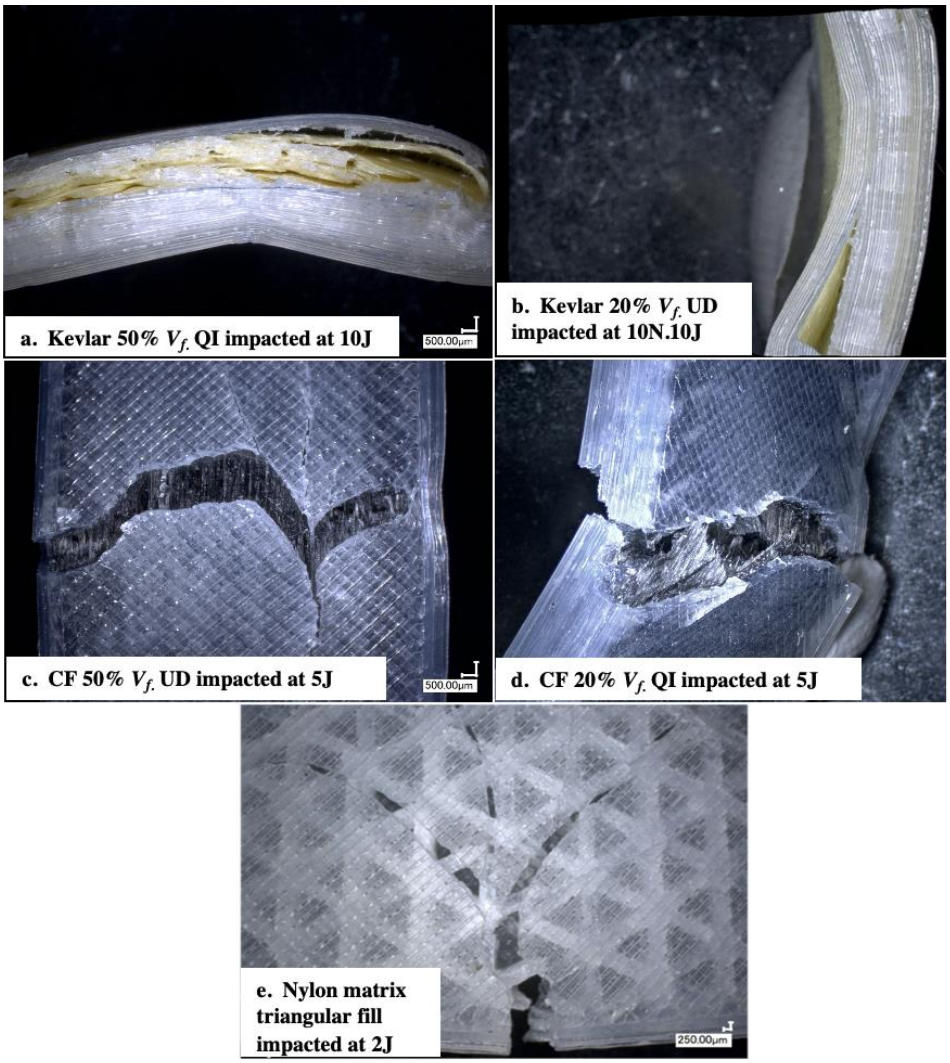

Figure 4 Failure modes of impacted samples

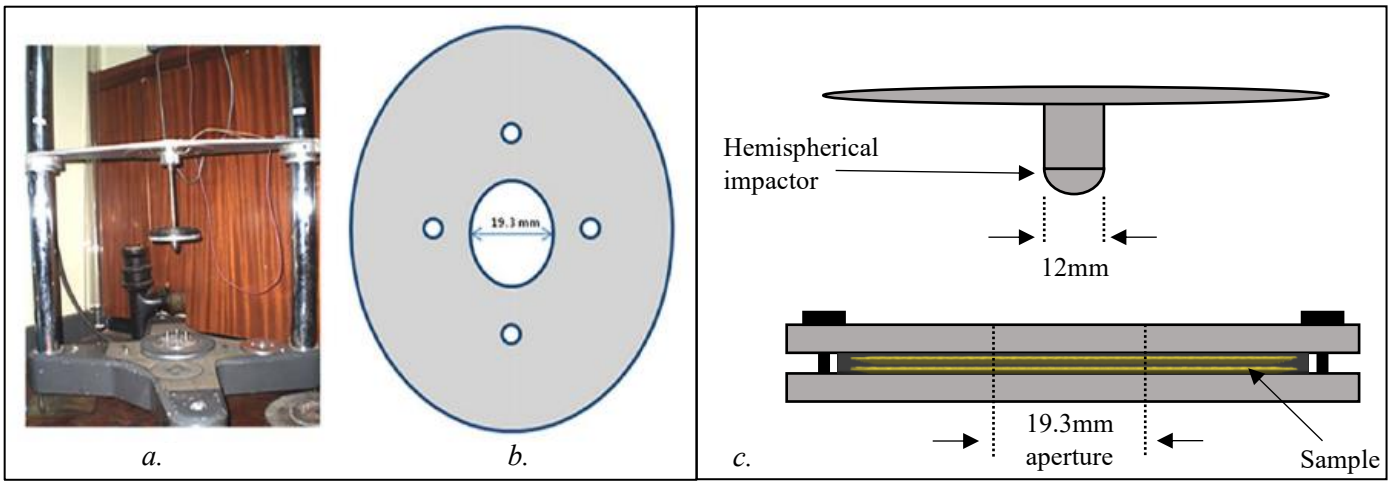

Figure 5 Weight-drop impactor (a) impact specimen support frame (b) Hemispherical impactor with support frame (c)

Table 6 Analysis of CF/nylon composites properties

CF/nylon composites		
	Averaged properties	
Material	**Flexural Modulus (MPa)**	**St Dev**
CF QI (20% $V_{f.}$)	2661.4	2610.4
CF QI (50% $V_{f.}$)	3913.1	2591.2
CF UD (20% V_f)	5414.4	4081.3
CF UD (50% V_f)	8630.9	5014.3
	Flexural strength (MPa)	**St Dev**
CF QI (20% $V_{f.}$)	68.2	53.3
CF QI (50% $V_{f.}$)	49.3	49.3
CF UD (20% V_f)	112.2	96.8
CF UD (50% V_f)	164.1	101.8
	Energy absorbed (J/m3)	**St Dev**
CF QI (20% $V_{f.}$)	1.2	0.7
CF QI (50% $V_{f.}$)	1.3	0.8
CF UD (20% V_f)	1.1	1.0
CF UD (50% V_f)	2.2	1.2

Table 7 Analysis of Kevlar/nylon composites properties

Kevlar/nylon composites		
	Averaged properties	
Material	**Flexural Modulus (MPa)**	**St Dev**
Kevlar QI (20% $V_{f.}$)	1009.6	372.1
Kevlar QI (50% $V_{f.}$)	1680.3	1007.4
Kevlar UD (20% V_f)	3305.1	1011.4
Kevlar UD (50% V_f)	5070.0	2382.3
	Flexural strength (MPa)	**St Dev**
Kevlar QI (20% $V_{f.}$)	34.6	20.1
Kevlar QI (50% $V_{f.}$)	22.1	8.9
Kevlar UD (20% V_f)	53.3	14.1
Kevlar UD (50% V_f)	88.1	36.7
	Energy absorbed (J/m3)	**St Dev**
Kevlar QI (20% $V_{f.}$)	1.3	0.7
Kevlar QI (50% $V_{f.}$)	1.3	0.7
Kevlar UD (20% V_f)	1.4	0.6
Kevlar UD (50% V_f)	2.2	1.3

Table 8 Passed and failed CF/nylon composites with their properties after being impacted until failure

Flexural Modulus (MPa)				
	Impact Energy			
Material	**0J**	**2J**	**5J**	**10J**
CF QI (20% V_f)	**6395.355**	**3807**	**443.427**	**Failed**
CF QI (50% V_f)	**7157.808**	**4877.282**	**3617.168**	**Failed**
CF UD (20% V_f)	**10362.224**	**8169.875**	**3125.535**	**Failed**
CF UD (50% V_f)	**12393.291**	**11257.565**	**10873.037**	**Failed**
Ultimate compressive strength (MPa)				
	Impact Energy			
Material	**0J**	**2J**	**5J**	**10J**
CF QI (20% V_f)	**129.603**	**109.927**	**33.363**	**Failed**
CF QI (50% V_f)	**150.64**	**74.021**	**98.695**	**Failed**
CF UD (20% V_f)	**197.409**	**218.876**	**32.831**	**Failed**
CF UD (50% V_f)	**279.435**	**195.227**	**181.821**	**Failed**
Absorbed Energy (J/m3)				
	Impact Energy			
Material	**0J**	**2J**	**5J**	**10J**
CF QI (20% V_f)	**1.88**	**1.96**	**1.04**	**Failed**
CF QI (50% V_f)	**2.16**	**1.11**	**1.98**	**Failed**
CF UD (20% V_f)	**2.62**	**1.66**	**0.45**	**Failed**
CF UD (50% V_f)	**3.16**	**2.84**	**2.97**	**Failed**

Table 9 Passed and failed Kevlar/nylon composites with their properties after being impacted until failure

Flexural Modulus (MPa)				
	Impact Energy			
Material	**0J**	**2J**	**5J**	**10J**
Kevlar QI (20% V_f.)	**1354.367**	**1194.342**	**383.801**	**1106.02**
Kevlar QI (50% V_f.)	**2685.799**	**2654.227**	**956.563**	**424.632**
Kevlar UD (20% V_f)	**4152.3**	**4397.98**	**1948.812**	**2721.504**
Kevlar UD (50% V_f)	**8504.633**	**5915.642**	**2212.269**	**3647.494**
Ultimate compressive strength (MPa)				
	Impact Energy			
Material	**0J**	**2J**	**5J**	**10J**
Kevlar QI (20% V_f.)	**67.008**	**24.083**	**13.331**	33.974
Kevlar QI (50% V_f.)	**84.057**	**85.357**	**22.097**	**22.098**
Kevlar UD (20% V_f.)	**68.325**	**65.244**	**34.095**	**45.881**
Kevlar UD (50% V_f.)	**151.004**	**74.564**	**57.681**	**69.405**
Absorbed (J/m3)				
	Impact Energy			
Material	**0J**	**2J**	**5J**	**10J**
Kevlar QI (20% V_f.)	**2.45**	**0.77**	**0.86**	**1.17**
Kevlar QI (50% V_f.)	**2.54**	**1.2**	**0.82**	**0.68**
Kevlar UD (20% V_f.)	**2.5**	**0.9**	**0.92**	**1.19**
Kevlar UD (50% V_f.)	**4.48**	**1.29**	**1.53**	**1.69**

Table 10 Passed and failed subjects of QI and UD fiber orientations

Impacted samples				
Materials	**Vf%**	**2J**	**5J**	**10J**
Kevlar isotropic UD	**LVF (20%)**	**Pass**	**Pass**	**Pass**
Kevlar isotropic UD	**HVF (50%)**	**Pass**	**Pass**	**Pass**
Kevlar QI	**LVF (20%)**	**Pass**	**Pass**	**Fail**
Kevlar QI	**HVF (50%)**	**Pass**	**Pass**	**Fail**
CF isotropic UD	**LVF (20%)**	**Pass**	**Pass**	**Fail**
CF isotropic UD	**HVF (50%)**	**Pass**	**Pass**	**Fail**
CF QI	**LVF (20%)**	**Pass**	**Pass**	**Fail**
CF QI	**HVF (50%)**	**Pass**	**Pass**	**Fail**

Under three-point bending prior to impact, when fibre-reinforced composite structures have all fibres acting perpendicular to an applied load, i.e., UD lay-up, tensile stresses are exerted on the opposing side of the applied stress. The tensile stress acts along the longitudinal fibres and as a result, it can withstand higher loads (Chawla, 1998b) . This behavior is noticeable in Figures 7-9. It indicates that 22UD Kevlar (50% $V_{f.}$) and 16UD CF (50% $V_{f.}$) samples at 0J have the highest flexural modulus, strength, and absorbed energy compared to the QI lay-up samples also at 0J. This is attributed to the strength of a UD printed composite. Unidirectional composites, in particular Kevlar fibres, are controlled by the buckling modes of fibres (on top of the sample where force is acting), specifically the buckling of individual fibres. If fibres were of a larger diameter, they would tend to exhibit greater resistance to local buckling and an increase to macroscopic failure. Therefore, the fibres in tension at the opposing side of the sample, will result in local fibrillation. The result is a greater stress underneath the sample in contrast to the top (Hull and Clyne, 1996).

The limitation of flexural properties witnessed with the lay-up of QI arises from the axisymmetric planes (45°/135° or +45°/-45° layers) which are exposed to shear stresses. Due to the various orientations of fibres, stress is distributed in the composite structure. As a result, fibres in the transverse direction (90°) or those in axisymmetric planes are significant contributors to the reduction in the maximum force (Mouritz, 2012). Fibre orientation plays a significant role in this instance showing that samples consisting of a QI lay-up present a lower storage modulus, strength, and absorbed energy (Figures 7-9).

After flexural testing, specimens experienced common failure modes, similarly, witnessed in conventional composites (Korkees, Allenby and Dorrington, 2020). Failure commenced when the bending or shear stresses became critical resulting in number of failure modes; fibre rupture, matrix cracking, micro-buckling and interlaminar shear cracking. When samples are impacted first and then flexural tested

similar failure modes occur, however, making failure more significant once flexural examination commenced. (Mouritz, 2012) (S. M.Fijul Kabir, Mathur and Seyam, 2020b).

Physical appearances between Kevlar samples and CF samples can be distinguished in Figure 6 after flexural testing. Interestingly, Kevlar samples produced opposing characteristics to CF samples in its flexural behaviour, as expected due to the results in Figures 7-9. Kevlar's distinct differences is due to its exceptional properties, which is high stiffness and high strength. These properties result from highly orientated chains extended along the fibre axis, with a resultant high modulus, subsequentially making it highly anisotropic (Chawla, 1998a). The nature of an aramid fibre consists of oriented para-substituted aromatic units, which make them rigid rod-like polymers (Fink, 2018). This makes Kevlar multi-fibrillar in its structure, and that's why it is exceedingly good at the absorption of energy. Its high aromaticity leads to an imbalance between its flexural strength and tensile strength. For this reason, its flexural properties are 20% of its tensile strength. However, weakness arises when Kevlar/nylon composites are in compression normal to the axis of applied stress, because fibres tend to form bands of buckling failure. (Johnston, Vaziri and Poursartip, 2001a).

Flexural failure imposed to the Kevlar samples was as a result of elastic deformation (of the strong covalent bonds). This only occurs to a limited degree before the weak van der Waals forces between the adjacent molecules are overcome and local fibrillation and damage occur (Hull and Clyne, 2012). Analysis of the charts, Figure 7-9 indicate Kevlar samples had a high-stress rupture life and exceedingly better fracture toughness than CF printed composites. However, due to its weak flexural properties, its strength could potentially be significantly lower than CF (Mallick, 2010). Upon incrementation of impact energies, flexural performance reduced across all samples, also seen with samples having a higher V_f%. (Figures 7-9). Therefore, tests performed, represented distinctly that the group of samples which only underwent flexural testing (0J) presented much higher values in all cases (strength, young's modulus, and AEUB).

Physical damage to the samples was also distinguishable between the different V_f% showing more prominent failure at CF 20%V_f. with visible matrix cracking (Figure 6a.) and no apparent matrix cracking for CF 50%V_f. in Figure 6c. This occurrence was because of the preceding damage generated in the samples from the drop-weight impact head (Figure 5c.). However, overall, the greatest flexural performance was that of the CF/nylon composite samples attributing to the higher specific stiffness of CFs. For this reason, energy absorption capabilities are potentially sacrificed which meant Kevlar/nylon composites had higher energy absorption capability (Figure 9).

Figure 6 Flexural tested samples before and after impact for carbon fibre and Kevlar reinforced nylon composites

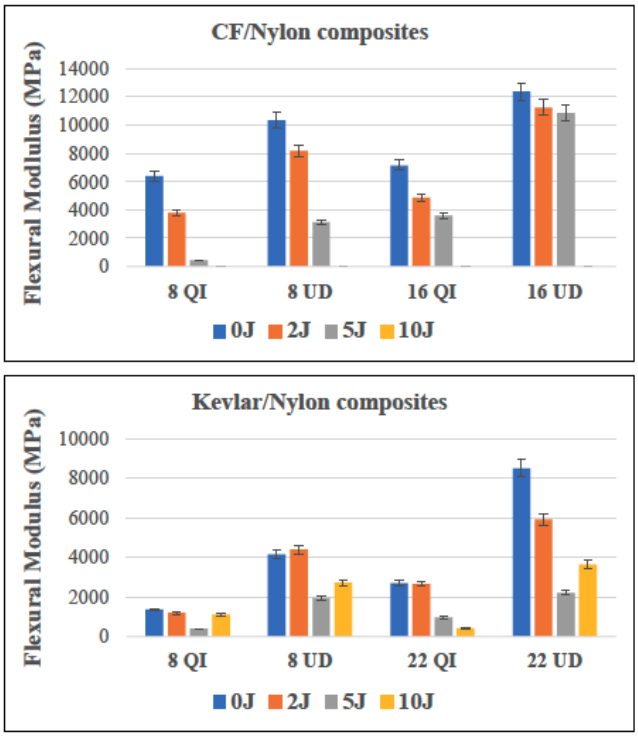

Figure 7 Flexural modulus comparison of all unimpacted and impacted 3D printed CF and Kevlar composites

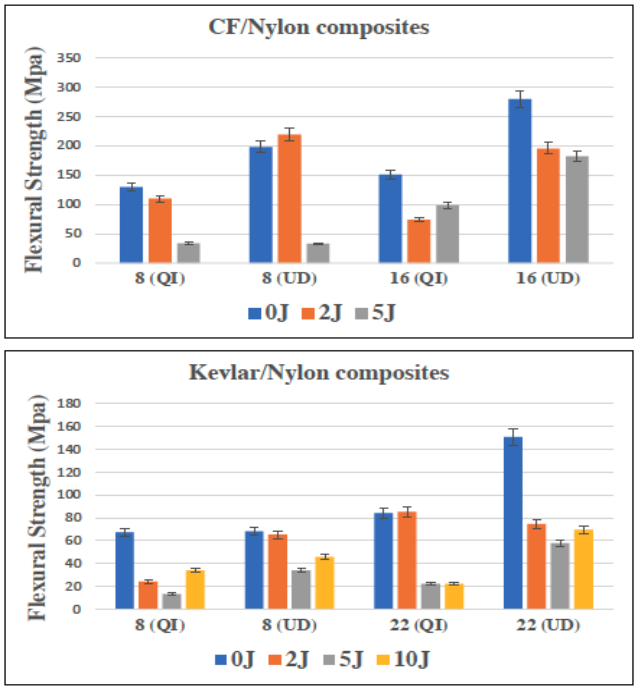

Figure 8 Flexural strength comparison of impact and unimpacted Kevlar and CF samples

3.4. Energy absorption before and after impact

Lay-up of fibres, and V_f% plays a critically important role in the amount of energy a composite can absorb, similarly seen by (Johnston, Vaziri and Poursartip, 2001b) and also exhibited in the results (Figure 9). Additionally seen by (S. M.Fijul Kabir, Mathur and Seyam, 2020a), without the inclusion of fibres in a nylon matrix the flexural modulus and absorbed energy of it is lower than if it had fibres as reinforcement. For the latter part, fibres would bear majority of the load during the period of impact, and once again being flexural tested after impact. This is in relation to, matrix cracking occurring first making the 3D printed FRPC structure rely greatly on the fibres alone. Hence, in no specific order, interface debonding of fibres, and fibre breakage would be the end result (Tan *et al.,* 2015). It is also important to note, low velocity impact results in undetectable damage which consequently means risk of potential microscopic failure points compared to high velocity impact (Jenq, Jing and Chung, 1994; Ghelli and Minak, 2011).

Interpreting the mentioned failure modes to the tests performed indicated that the group which was impact tested first followed by flexural testing resulted in lower AEUB (Figure 9). It demonstrated that composites possessing multiple failure modes before undergoing flexural testing made the composite weaker. In addition, microscopic defects might have initiated during 3D printing i.e., voids, and so was detrimental to the composite properties before being impacted or flexural tested. As a result, energy absorption capabilities are adversely affected. Analysis of the AEUB chart (Figure 9) revealed Kevlar 50% V_f (UD), had the highest absorbed energy under bending (AEUB) out of all tested samples (4.48Jm-3), followed by CF 50% V_f (UD) (3.16Jm-3). However, Kevlar showed to be the most effected by damage imposed to the structure. This was indicated by the large reduction in AEUB when impact energy increased. Similarly, CF/nylon samples had the same effect but on a smaller scale (Figure 9). The reduction of values obtained was seen because AEUB is influenced by the boundary condition of low velocity impact and duration of impact. The impact duration is long enough for the entire composite structure to respond and react to the impact, and due to fibre preform architecture, significant influence over the impact mode of the composites can occur and alterations to the boundary conditions for the impact response can be made (Davies, Hitchings and Wang, 2000). Therefore, it can be seen that the higher the impact energy the more noticeable the damage to fibres is, therefore, the more damaged the composite is as a whole (Figures 4e. and 4d.). This results in a higher reduction of residual AEUB when undergoing flexural testing. Additionally, insufficient amount of nylon matrix is capable of working coherently with fibres to support the acting load causing this phenomenon. However, a clear elaboration of the residual AEUB (Figure 9) displays that a lay-up of UD at a 50% V_f, was the most suitable composite structure for sufficient AEUB. Those with the higher V_f % showed higher attained values than 3D printed FRPC structures with a lower V_f% and a lay-up of QI.

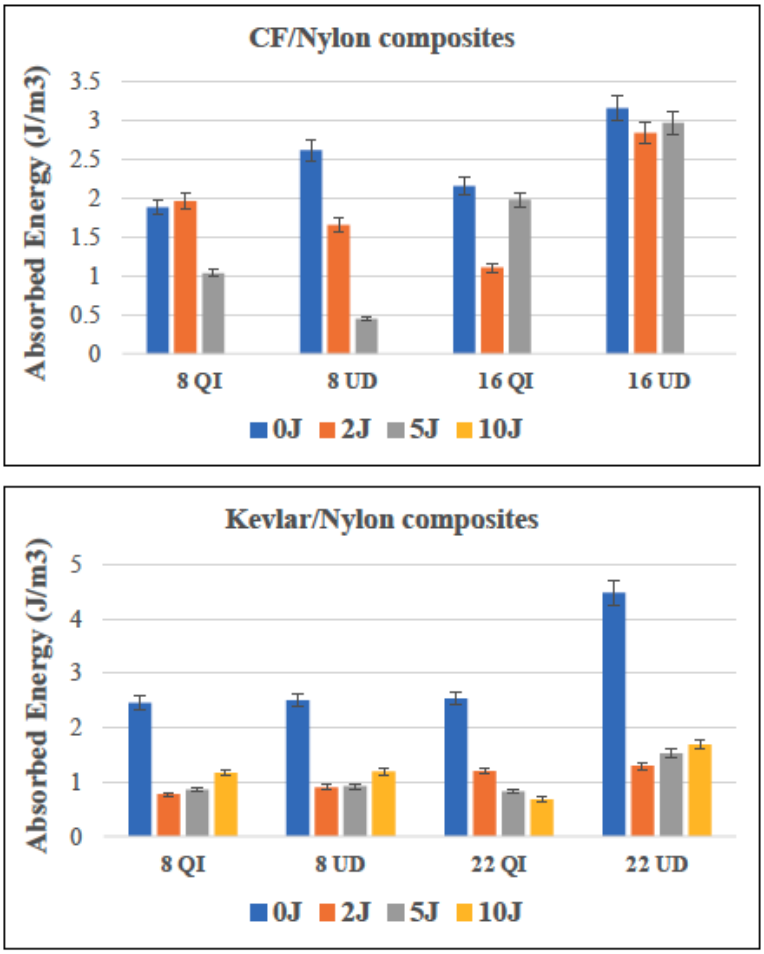

Figure 9 Absorbed energy under bending for all impacted and unimpacted 3D printed CF and Kevlar composites

3.5 The effects of temperature on impact and flexural performance of 3D printed UD FRPC's

An investigation into the effect of temperature on the composite structures was done, and due to the advantages provided by continuous concentric fibres (Mei *et al.,* 2019), a concentric fill pattern with CF as reinforcement was utilized, Figure 1. The sub-ambient temperatures were also performed on short fibres (Onyx). This permitted for comparison of short fibres and continuous fibres at different temperature regimes. The difference in flexural values between the two temperature regimes are exhibited in Figures 10-12.

Important to note, under cryogenic temperatures, nylon will become increasingly hard, stiff and brittle in response to mechanical loads. This could work coherently with the higher molecular weight superiority of nylon as shown under cold conditions. Additionally, since amorphous polymers lack structured regions, under sub-ambient conditions the randomly orientated chains become less mobile, and increase in rigidity, increasing the resistance to plastic deformation, and therefore improving stiffness modulus (Hechtel, 2014). This is seen in Figure 10, indicating that samples tested at LT provided higher flexural modulus. Consequently, an increase in stiffness and brittleness of the nylon matrix adversely effects

the CF/nylon composites when impacted. Results for this is tabulated as a matrix in Tables 11 and 12 indicating those which have passed/failed under the energy impacted. Therefore, an earlier failure at LT CF/nylon (Table 12) for both Vf% occurred in comparison to the RT samples (Table 11). On the contrary, it can be observed from Tables 11 and 12 that CF/nylon printed composites, nylon, and Onyx displayed a considerable increase in flexural modulus compared to flexural and impact tests performed at RT. This exhibits a typical cryogenic behavior most polymers follow. However, it can be seen from Figures 10 and 11 that the flexural properties of all specimens decreased at both environments RT and LT with incrementation of impact energies (2-8J).

In the case of continuous fibres and discontinuous fibres (short fibres/Onyx), Onyx is distinguishable to CF/nylon composites. Therefore, it is necessary to expand on it. Onyx contains discontinuous/short carbon fibres which enhance its stiffness. These fibres are randomly orientated, and so make them isotropic resulting in high properties but not as high if the fibres were orientated in the longitudinal direction as continuous fibres (Callister Jr. and Rethwisch, 2019). Therefore, Onyx as a short CF reinforced nylon composite showed a greater flexural modulus (930.35MPa) at RT compared to nylon (490.49MPa) (Table 11). Consequently, it produces a lower modulus compared to continuous CF/nylon composite (5894.44MPa at 20% V_f and 11185.38MPa at 50% V_f) seen in Table 11. The length of the reinforcing fibre in this case is vital for the impact resistance of the printed composites since the continuous fibre reinforced samples could resist higher impact energies compared to nylon and Onyx (Callister Jr. and Rethwisch, 2019). This being said, it was evident that as impact energies increased more abrupt failure occurred for the Onyx, nylon, and CF/nylon 20% V_f. However, analyzing the behaviour of 50% V_f CF/nylon at RT (Table 11), it can be noted that it successfully passed all impact energies without complete failure. Therefore, fibre volume fraction played a substantially important role influencing the outcome of results. The higher Vf% composite was the optimum sample with the highest values for all properties compared to 20% V_f CF/Nylon printed composite, Onyx, and nylon. A statistical analysis helps to distinguish the differences in flexural properties between the two temperature regimes in Table 13 and Table 14. The flexural properties and energy absorbed results were averages to determine the standard deviation. It indicated that samples flexural tested and impacted at RT produced results close to the mean, presenting suitable signs of close dispersion. Therefore, more consistent results were seen in comparison to samples tested at LT.

Not only does the length of the fibre in the composite affect the impact resistance and flexural properties, but the lay-up/fibre orientation does as well. The work produced by (Morioka and Tomita, 2000) demonstrated that unidirectional long CF/epoxy composites with a smaller angle between fibres and direction of the specimen length independent of the composite type had a high bending fracture energy as well as high strength (Morioka and Tomita, 2000). However, the composite displayed remarkable anisotropy in their fracture energy as the angle increased. Whereas the isotropy of mechanical properties is much more suited to structural components due to the expected loading with ply orientations to be in different directions (Morioka and Tomita, 2000). This displays the important connection between design, lay-up, and properties.

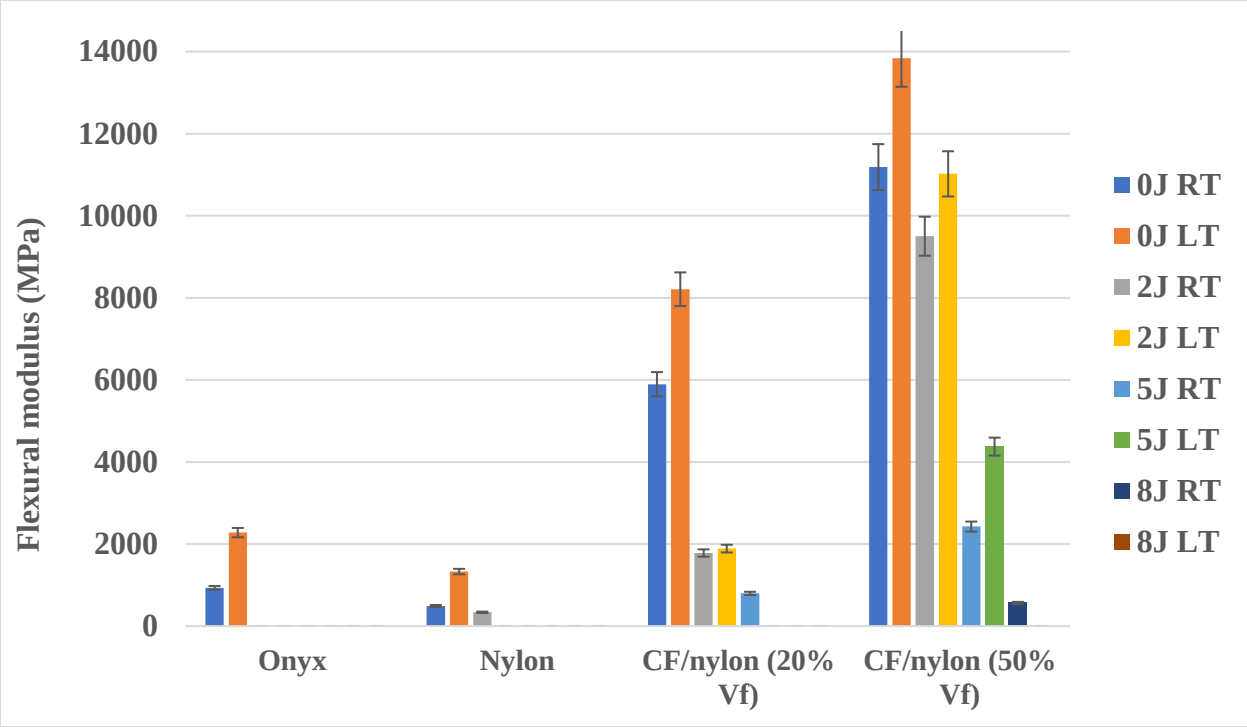

Figure 10 Flexural modulus of samples impacted at cumulating impact energies and different temperature regimes to compare concentric UD CF fibre fill patterns at both volume fractions to Onyx and Nylon

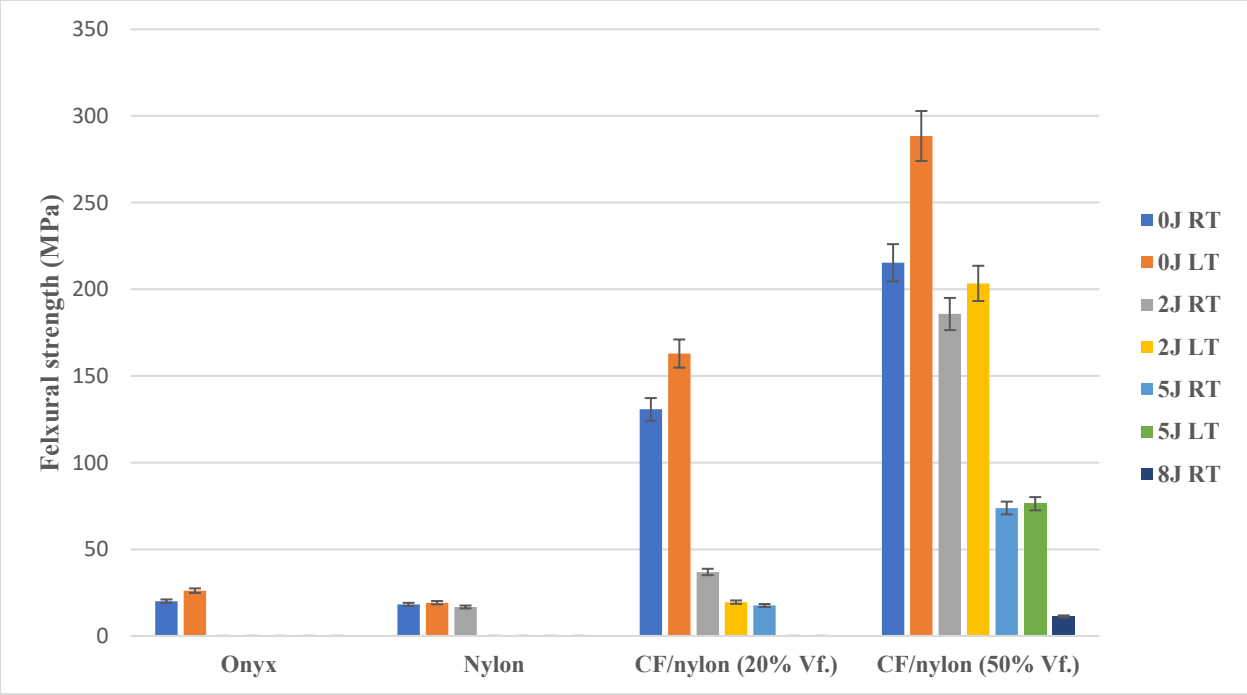

Figure 11 Flexural strength of samples impacted at cumulating impact energies and different temperature regimes to compare concentric UD CF fibre fill patterns at both volume fractions to Onyx and Nylon

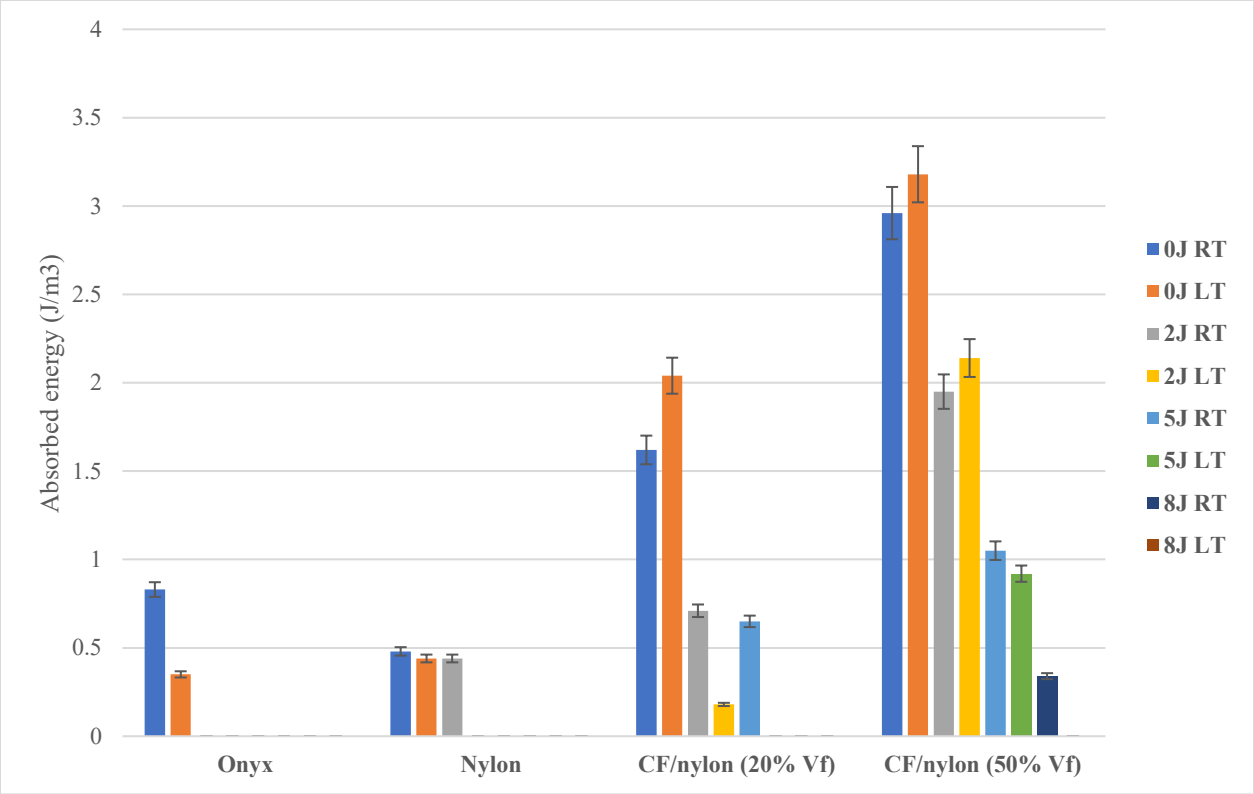

Figure 12 Absorbed energy of samples impacted at cumulating impact energies and different temperature regimes to compare concentric UD CF fibre fill patterns at both volume fractions to Onyx and Nylon

Table 11 Passed and failed CF/nylon composites, Onyx, and nylon with their properties after being impacted until failure

Flexural Modulus (MPa)				
	Impact Energy			
Material	**0J**	**2J**	**5J**	**8J**
Onyx	**930.35**	**Failed**	**Failed**	**Failed**
Nylon	**490.49**	**336.89**	**Failed**	**Failed**
CF (20% V_f.)	**5894.44**	**1781.18**	**796.87**	**Failed**
CF (50% V_f.)	**11185.38**	**9501.66**	**2425.88**	**562.59**
Ultimate compressive strength (MPa)				
	Impact Energy			
Material	**0J**	**2J**	**5J**	**8J**
Onyx	**20.05**	**Failed**	**Failed**	**Failed**
Nylon	**18.2**	**16.71**	**Failed**	**Failed**
CF (20% V_f.)	**130.7**	**36.89**	**17.54**	**Failed**
CF (50% V_f.)	**215.27**	**185.72**	**73.81**	**11.26**
Absorbed energy under bending (J/m3)				
	Impact Energy			
Material	**0J**	**2J**	**5J**	**8J**
Onyx	**0.83**	**Failed**	**Failed**	**Failed**
Nylon	**0.48**	**0.44**	**Failed**	**Failed**
CF (20% V_f.)	**1.62**	**0.71**	**0.65**	**Failed**
CF (50% V_f.)	**2.96**	**1.95**	**1.05**	**0.34**

Table 12 Passed and failed CF/nylon composites, Onyx, and nylon with their properties after being impacted until failure

Flexural Modulus (MPa)				
	Impact Energy			
Material	**0J**	**2J**	**5J**	**8J**
Onyx	**2278.28**	**Failed**	**Failed**	**Failed**
Nylon	**1328.50**	**Failed**	**Failed**	**Failed**
CF (20% V_f.)	**8208.95**	**1888.07**	**Failed**	**Failed**
CF (50% V_f.)	**13833.84**	**11020.3**	**4374.17**	**Failed**
Ultimate compressive strength (MPa)				
	Impact Energy			
Material	**0J**	**2J**	**5J**	**8J**
Onyx	**26.12**	**Failed**	**Failed**	**Failed**
Nylon	**19.18**	**Failed**	**Failed**	**Failed**
CF (20% V_f.)	**162.9**	**19.48**	**Failed**	**Failed**
CF (50% V_f.)	**288.45**	**203.39**	**76.28**	**Failed**
Absorbed energy under bending (J/m3)				
	Impact Energy			
Material	**0J**	**2J**	**5J**	**8J**
Onyx	**0.35**	**Failed**	**Failed**	**Failed**
Nylon	**0.44**	**Failed**	**Failed**	**Failed**
CF (20% V_f.)	**2.04**	**0.18**	**Failed**	**Failed**
CF (50% V_f.)	**3.18**	**2.14**	**0.92**	**Failed**

Table 13 Analysis of subject's properties tested at room temperature

Samples tested at RT		
	Averaged properties	
Material	**Flexural Modulus (MPa)**	**St Dev**
Onyx	232.5	402.8
Nylon	206.8	213.8
CF (20% V*f*)	2118.1	2269.7
CF (50% V*f*)	5918.8	4512.8
	Flexural strength (MPa)	**St Dev**
Onyx	5.0	8.6
Nylon	8.7	8.7
CF (20% V*f*)	46.2	50.4
CF (50% V*f*)	121.5	82.6
	Energy absorbed (J/m3)	**St Dev**
Onyx	0.2	0.3
Nylon	0.2	0.2
CF (20% V*f*)	0.7	0.5
CF (50% V*f*)	1.5	0.9

Table 14 Analysis of subject's properties tested at low temperature

Samples tested at LT		
	Averaged properties	
Material	**Flexural Modulus (MPa)**	**St Dev**
Onyx	569.5	986.5
Nylon	332.1	575.2
CF (20% V*f*)	2524.2	3371.3
CF (50% V*f*)	7307.0	5440.1
	Flexural strength (MPa)	**St Dev**
Onyx	6.5	11.3
Nylon	4.7	8.3
CF (20% V*f*)	45.5	68.1
CF (50% V*f*)	142.0	111.4
	Energy absorbed (J/m3)	**St Dev**
Onyx	0.1	0.15
Nylon	0.1	0.19
CF (20% V*f*)	0.5	0.8
CF (50% V*f*)	1.5	1.2

3.6 The effects of temperature on the energy absorption capabilities of 3D printed UD FRPCs

Evidently, temperature had a noticeable effect on the properties of the CF/nylon composites consisting of concentric rings seen in previous Figures 10-12. An increase of energy absorption occurred when they were exposed to LT (Figure 12), with supported data also shown in Tables 11 and 12. On the contrary, Onyx and nylon reduced in AEUB with the reduction in temperature (Figure 12). Results showed 50% V_f CF tested at LT consisting of CF concentric rings exhibited a value of 3.18Jm^{-3}. In comparison to Onyx, nylon and CF/nylon 20% V_f samples, produced lower AEUB.

Therefore, it is understood that Onyx and nylon experienced a decrease in their ability to withstand the amount of energy imposed as temperature regimes reached sub-ambient temperatures. The HVF samples indicated that as temperatures reduced absorbed energy increased in comparison to LVF samples. This opposing behaviour arises because LVF samples contained a higher P*v* (Table 5). Therefore, LVF composites, Onyx and nylon behaved in this manner as a result of an increase in brittleness approaching

sub-ambient temperatures, and a larger volume of nylon. The brittleness of Onyx was clear in both temperature regimes as complete failure occurred at LT for any energy at 2J or above (Tables 11 and 12). Thus, this brittleness of Onyx related to why it experienced a lower AEUB when placed at LT. Nylon showed a similar behvaiour yet on a smaller scale. It passed the impact test at 2J for RT but failing at 2J for LT expressing the effect of temperature negatively effecting the ductile nature of nylon.

To elaborate, the brittle behaviour develops across all samples because, at LT the matrix behaviour dominates, and the material hardens up, becoming stiff and brittle/more brittle (Dutta and Hui, 1996). This determines the dominate flexural behaviour of the matrix and leads to an increase of the modulus, ultimate stress and energy absorbed at LT. Due to the temperature change, the composites flexural properties were controlled. Therefore, if impact energies increase at sub-ambient temperatures the matrix would not be capable of withstanding the same amount of impact energy as at RT, i.e., less than RT. This was seen in Tables 11 and 12 where a reduction in properties was noticed, in addition to a reduction of AEUB in Figure 12. It was similarly studied by (Shonaike, 1988) showing that the fracture behaviour of nylon is brittle when tested at temperatures below (-150°).

Energy absorption can be significantly affected by the failure modes of the CF/nylon composites studied. Failure modes like, microcracking within the matrix and matrix-fibre interfaces might occur due to the difference in the thermal expansion of both nylon and CFs once printed. This could lead to harmful residual stresses in the composite structure negatively affecting its properties (Kichhannagari, 2004). A clearer representation of these failure modes is expressed in Figure 13. Interestingly, the samples in Figure 13 were impacted at the lowest impact energy, yet the damage was distinct and apparent. Additionally, damage in the HVF samples (Figure 13b. and c.) seemed worse than LVF samples (Figure13a. and d.) due to the likelihood of residual stresses, like voids, more commonly experienced with a higher CF content.

In contrast to LT samples (Figure 14), samples at RT had a matrix acting in a ductile manner, aiding in flexibility and allowing for the composite to attain its properties at higher impact energies. At impact energies 2-8J at RT in Figure 14, complete structural failure wasn't exhibited but the composites experienced extensive surface and internal damage, i.e., micro-cracking which led to a reduction in flexural properties. It was noticeable that crack propagation had occurred to nylon without the inclusion of CFs (Figure 14a.). This exposes the attributes of fibres used as reinforcement. Upon impact, stresses would be distributed throughout the fibres rather than the matrix alone, if fibres were used, reducing the significance of matrix crack propagation *(Luo* et al.*, 2019)*. Therefore, the main failure modes observed for the majority of the samples in both temperature environments was matrix cracking, fibre fracture, delamination and fibre-matrix interface debonding which are the most common failures in composite materials (Opelt, Cândido and Rezende, 2018).

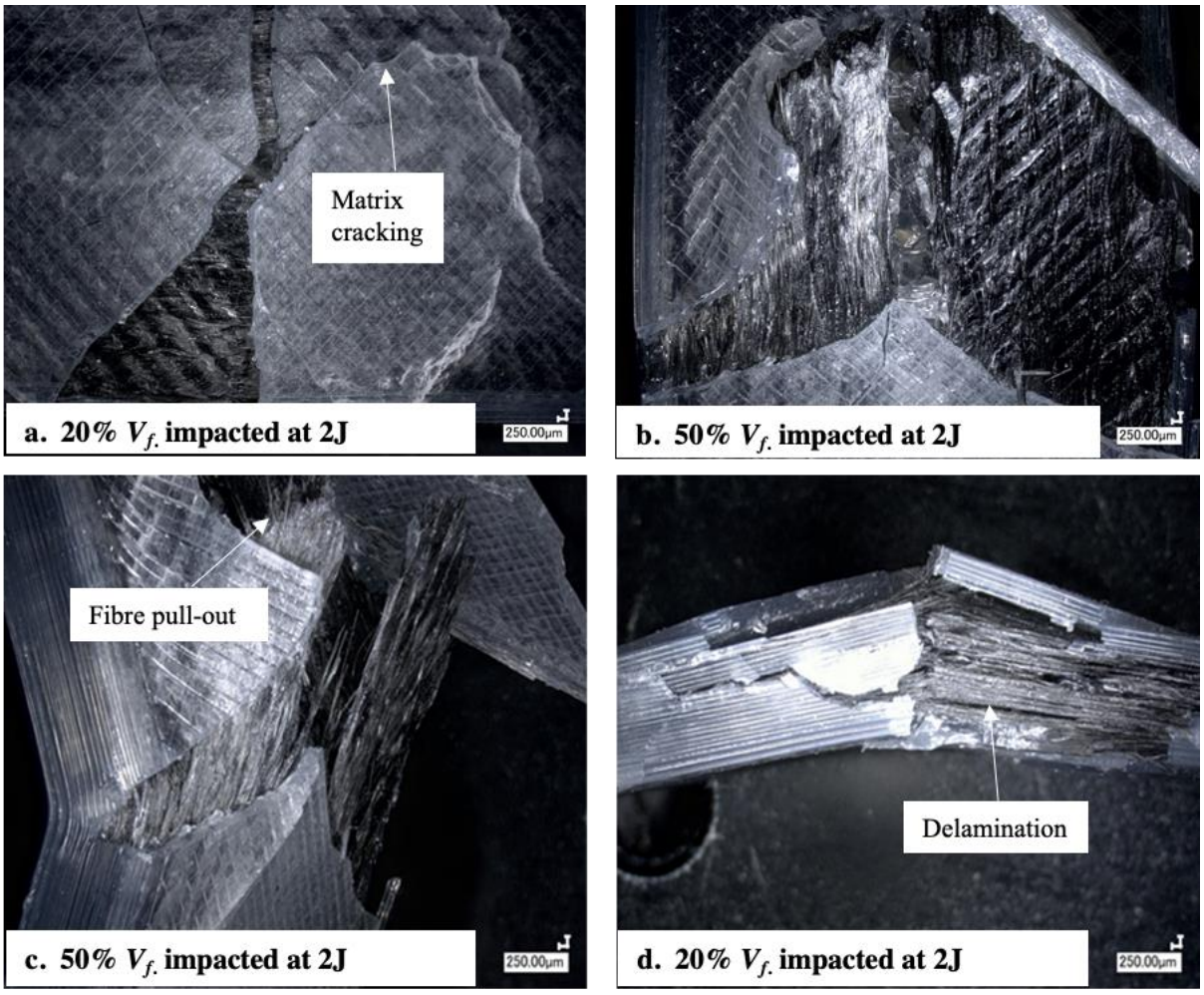

Figure 13 Samples impacted at low temperature where LVF 20% samples are (a.) and (d.) concentric CF /nylon samples, and HVF 50% are (b.) and (c.) concentric CF/nylon samples.

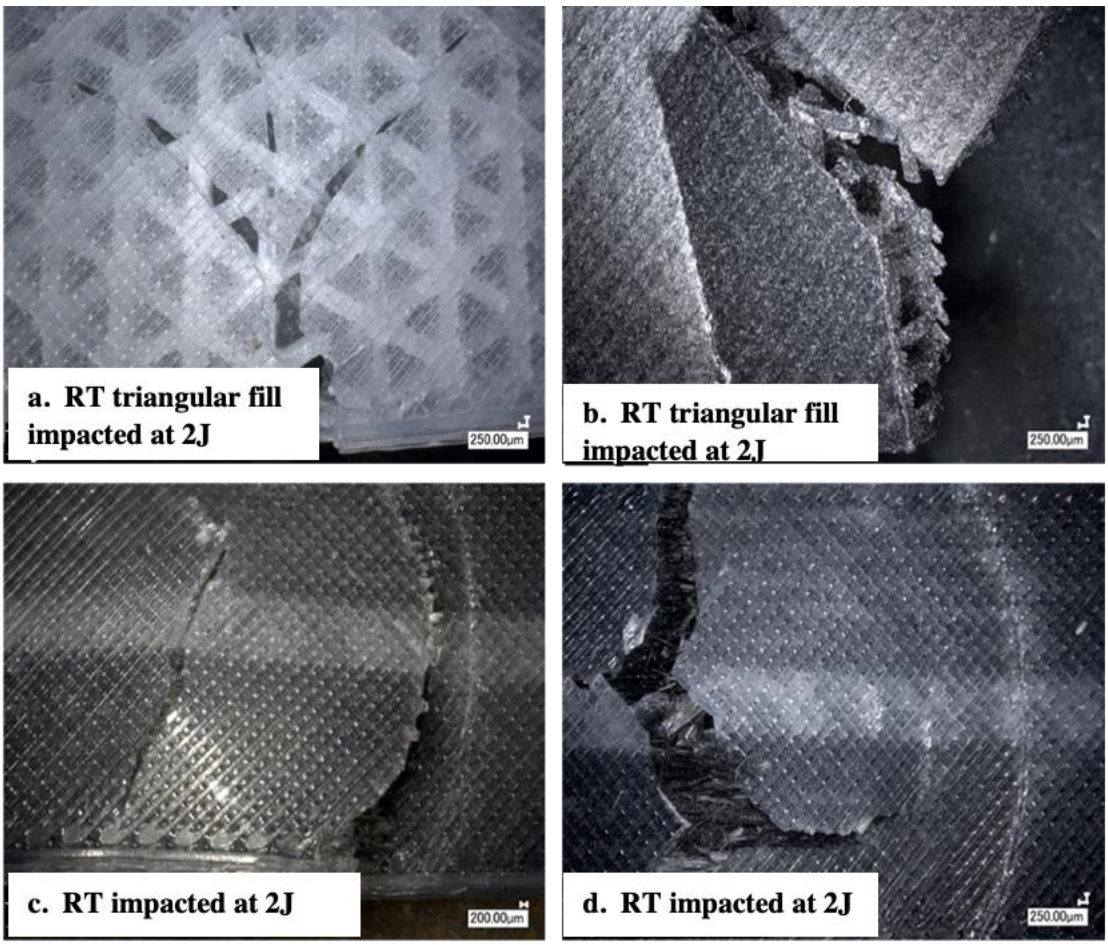

Figure 14 Impacted samples, (a) Nylon with fill density of 50% and triangular fill pattern, (b) Onyx with fill density of 50% and triangular fill pattern, (c) CF LVF 20% $V_{f.}$ in UD concentric pattern, and (d) CF HVF 50% $V_{f.}$ in UD concentric pattern

1.4 Conclusion

An investigation into the impact behaviour and flexural residual properties of 3D printed FRPCs was studied at both RT and LT temperature regimes by drop-weight impact testing and three-point bend testing. Continuous carbon and Kevlar fibre reinforced nylon composites as well as short carbon fibre/nylon composites (Onyx) were printed and tested. Impact properties, residual flexural strength, flexural modulus, and AEUB were the main parameters to be analyzed. Aspects considered was the lay-up orientation of fibres, fibre volume fraction and fibre type.

It was observed that V_f.% had a positive influence on the composites. Printed specimens with 50% V_f. improved the mechanical performance of the composite and showed better impact and residual flexural properties in comparison to 20% V_f. This is coupled with the best fibre orientation, i.e., concentric, and fibre nature (CF/nylon) for optimum flexural modulus, and flexural strength when the samples were not impacted at LT. However, Kevlar/nylon composites provided the most optimum energy absorption properties.

After impact, High depth of field imaging showed Kevlar experienced a common failure mode known as Euler buckling of individual fibres as well as kinking band formations. Whereas, CF/nylon composites (both concentric, UD and QI) experienced matrix cracking, delamination, fibre pull-out and fibre fracture which occurred at both temperature regimes. On the contrary, Onyx experienced matrix cracking and catastrophic failure, also at both temperature regimes.

In general, the flexural properties of all printed composites decreased with increasing impact energy due to the potential increase of failure modes. The failure behavior of all was dominated by delamination, matrix cracking and fibre fracture. It was clear that matrix cracking was more apparent in most of the samples. This is largely related to the matrix bearing most of the load and experiencing macroscopic damage since it has a lower modulus and strength than the fibres. Consequently, the matrix experienced more stress with the reduction of temperature at LT, causing more abrupt failure of all samples at that temperature regime due to the increase of brittleness.

Furthermore, it can be concluded out of the QI and UD samples, that printed Kevlar/nylon composites exhibited greater resistance to impact and thus had greater flexural performance than printed CF/nylon composites. Kevlar fibres exhibited higher plastic deformation occurring over a longer period, thus having higher strain-to-failure. In terms of stiffness and strength, CF/nylon showed more superior results in its flexural properties. However, Kevlar/nylon composites had standard deviation (σ) values further below the mean value indicating an inconsistency of values obtained for all Kevlar lay-ups after impact.

Moreover, the flexural properties of all printed samples unimpacted (0J) tested at sub-ambient temperatures slightly improved compared to those at RT. This can be attributed to the increase in the rigidity of the nylon matrix which in turn improved the flexural performance of the specimens but with a more catastrophic failure to it. Furthermore, samples flexural tested and impacted at RT produced results close to the mean, presenting suitable signs of close dispersion. Therefore, more consistent results were seen in comparison to samples tested at LT.

Impacting all short and continuous carbon fibre/nylon composites at LT led to a reduction in all residual flexural properties of the samples with incrementation of impact energy. This was because the nylon matrix became more brittle at LT and thus further damage was generated in the materials when impacted at various impact energies. However, UD 50% V_f. CF/nylon printed composites exhibited the best flexural properties before and after impact at both temperature regimes. This demonstrates the benefits of Vf% and fibre orientation, and the influence it has over the composite properties.

References:

Agarwal, K. et al. (2018), “Mechanical properties of fiber reinforced polymer composites: a comparative study of conventional and additive manufacturing methods”, Journal of Composite Materials, Vol. 52 No. 23, pp. 3173-3181, doi:10.1177/0021998318762297.

AlOmari, A.S. et al. (2020), “Experimental and computational analysis of Low-Velocity impact on carbon-, glass- and Mixed-Fiber composite plates”, Journal of Composites Science, Vol. 4 No. 4, p. 148, doi: 10.3390/JCS4040148.

Araya-Calvo,M. et al. (2018), “Evaluation of compressive and flexural properties of continuous fiber fabrication additive manufacturing technology”, Additive Manufacturing, Vol. 22, pp. 157-164, doi: 10.1016/J.ADDMA.2018.05.007.

Benavidez, A.D. et al. (2019), “Mechanical properties of carbon and glass fibre reinforced composites produced by additive manufacturing: a short review”, IOP Conference Series: Materials Science and Engineering, Vol. 670 No. 1, p. 12020, doi: 10.1088/1757-899X/670/1/012020.

British Standards Institution. and International Organization for Standardization (2011), “Fibre-reinforced plastic composite: determination of flexural properties”, p. 16, available at: www.en-standard.eu/bs-en-iso-14125-1998-a1- 2011-fibre-reinforced-plastic-composites-determination of flexural-properties/ (accessed 4 February 2022).

Callister, W.D., Jr. and Rethwisch, D.R. (2019), “Callister’s Materials Science and Engineering, 10th ed., Global Edition,” p. 944.

Caminero, M.A. et al. (2018), “Impact damage resistance of 3D printed continuous fibre reinforced thermoplastic composites using fused deposition modelling”, Composites Part B: Engineering, Vol. 148, pp. 93-103, doi: 10.1016/J. COMPOSITESB.2018.04.054.

Caz on-Martín, A. et al. (2019), “Design and manufacturing of shin pads with multi-material additive manufactured features for football players: a comparison with commercial shin pads”, Proceedings of the Institution of Mechanical Engineers, Part P: Journal of Sports Engineering and Technology, Vol. 233 No. 1, pp. 160-169, doi: 10.1177/1754337118811266.

Chawla, K.K. (1998a), “Polymer matrix composites”, in Composite Materials, Springer, New York, NY, pp. 133-163, doi: 10.1007/978-1-4757-2966-5_5.

Chawla, K.K. (1998b), “Reinforcements”, in Composite Materials, Springer New York, NY, pp. 6-71, doi: 10.1007/ 978-1-4757-2966-5_2.

Davies, G.A.O., Hitchings, D. and Wang, J. (2000), “Prediction of threshold impact energy for onset of delamination in quasi-isotropic carbon/epoxy composite laminates under low-velocity impact”, Composites Science and Technology, Vol. 60 No. 1, pp. 1-7, doi: 10.1016/S0266-3538 (99)00092-5.

Dickson, A.N. et al. (2017), “Fabrication of continuous carbon, glass and kevlar fibre reinforced polymer composites using additive manufacturing”, Additive Manufacturing, Vol. 16, pp. 146-152, doi: 10.1016/J.ADDMA. 2017.06.004.

Dutta, P.K. and Hui, D. (1996), “Low-temperature and freeze-thaw durability of thick composites”, Composites Part B: Engineering, Vol. 27 Nos 3/4, pp. 371-379, doi: 10.1016/ 1359-8368(96)00007-8.

Fink, J.K. (2018), “3D industrial printing with polymers, 3D industrial printing with polymers”, doi:10.1002/978111 9555308.

Flansburg, B.D., Engelstad, S.P. and Rousseau, C.Q. (2010), “A probabilistic study of composite impact damage design strain allowables”, Collection of Technical Papers - AIAA/ ASME/ASCE/AHS/ASC Structures, Structural Dynamics and Materials Conference [Preprint], doi: 10.2514/6.2010-2866.

Ghelli, D. and Minak, G. (2011), “Low velocity impact and compression after impact tests on thin carbon/epoxy laminates”, Composites Part B: Engineering, Vol. 42 No. 7, pp. 2067-2079, doi: 10.1016/J.COMPOSITESB. 2011.04.017.

Goh, G.D. et al. (2017), “Characterization of mechanical properties and fracture mode of additively manufactured carbon fiber and glass fiber reinforced thermoplastics”, doi: 10.1016/j.matdes.2017.10.021.

Hosseinzadeh, R., Mehrdad Shokrieh, M. and Lessard, L. (2005), “Damage behavior of fiber reinforced composite plates subjected to drop weight impacts”, doi: 10.1016/j. compscitech.2005.05.025.

Howard, J.D. et al. (2020), “Evaluating additive manufacturing for the production of custom head supports: a comparison against a commercial head support under static loading conditions”, Proceedings of the Institution of Mechanical Engineers, Part H: Journal of Engineering in Medicine, Vol. 234 No. 5, pp. 458-467, doi: 10.1177/0954411919899844.

Hull, D. and Clyne, T.W. (1996), An Introduction to Composite Materials, an Introduction to Composite Materials, Cambridge University Press, doi: 10.1017/cbo9781139170130.

Hull, D. and Clyne, T.W. (2012), “Strength of composites”, in An Introduction to Composite Materials, Cambridge University Press, pp. 158-207, doi: 10.1017/cbo9781139170130.010.

Jenq, S.T., Jing, H.S. and Chung, C. (1994), “Predicting the ballistic limit for plain woven glass/epoxy composite laminate”, International Journal of Impact Engineering, Vol. 15 No. 4, pp. 451-464, doi: 10.1016/0734-743X(94)80028-8.

Johnston, A., Vaziri, R. and Poursartip, A. (2001), “A plane strain model for Process-Induced deformation of laminated composite structures”, Journal of Composite Materials, Vol. 35 No. 16, pp. 1435-1469, doi: 10.1106/YXEA-5MH9-76J5-BACK.

Kabir, S.M.F., Mathur, K. and Seyam, A.F.M. (2020a), “A critical review on 3D printed continuous fiber-reinforced composites: history, mechanism, materials and properties”, Composite Structures, Vol. 232, p. 232, doi: 10.1016/J. COMPSTRUCT.2019.111476.

Kabir, S.M.F., Mathur, K. and Seyam, A.F.M. (2020b), “Impact resistance and failure mechanism of 3D printed continuous fiber-reinforced cellular composites”, The Journal of the Textile Institute, Vol. 112 No. 5, pp. 752-766, doi: 10.1080/00405000.2020.1778223.

Kabir, S.M.F., Mathur, K. and Seyam, A.-F.M. (2020c), “The road to improved Fiber-Reinforced 3D printing technology”, Technologies, Vol. 8 No. 4, p. 51, doi: 10.3390/ TECHNOLOGIES8040051.

Kabir, S.M.F., Mathur, K. and Seyam, A.-F.M. (2021), “Maximizing the performance of 3D printed Fiber- Reinforced composites”, Journal of Composites Science, Vol. 5 No. 5, p. 136, doi: 10.3390/JCS5050136.

Kichhannagari, S. (2004), “Effects of extreme low temperature on composite materials”, Undefined [Preprint].

Korkees, F., Allenby, J. and Dorrington, P. (2020), “3D printing of composites: design parameters and flexural performance”, Rapid Prototyping Journal, Vol. 26 No. 4, pp. 699-706, doi: 10.1108/RPJ-07-2019-0188.

Korkees, F., Arnold, C. and Alston, S. (2018), “Water absorption and low-energy impact and their role in the failure of 645° carbon fibre composites”, Polymer Composites, Vol. 39No. 8, pp. 2771-2782, doi: 10.1002/pc.24269.

Luo, M. et al. (2019), “Impregnation and interlayer bonding behaviours of 3D-printed continuous carbon-fiber reinforced poly-ether-ether-ketone composites”, Composites Part A: Applied Science and Manufacturing, Vol. 121, pp. 130-138, doi: 10.1016/J.COMPOSITESA.2019. 03.020.

Mallick, P.K. (2010), “Thermoplastics and thermoplasticmatrix composites for lightweight automotive structures”, in Materials, Design and Manufacturing for Lightweight Vehicles, Elsevier Ltd., pp. 174-207, doi: 10.1533/9781845 697822.1.174.

Mei, H. et al. (2019), “Tailoring strength and modulus by 3D printing different continuous fibers and filled structures into composites”, Advanced Composites and Hybrid Materials, Vol. 2 No. 2, pp. 312-319, doi: 10.1007/S42114-019- 00087-7.

Morioka, K. and Tomita, Y. (2000), “Effect of lay-up sequences on mechanical properties and fracture behavior of CFRP laminate composites”, Materials Characterization, Vol. 45 No. 2, pp. 125-136, doi: 10.1016/S1044-5803(00) 00065-6.

Mouritz, A.P. (2012), “Introduction to aerospace materials”, Introduction to Aerospace Materials, [Preprint]. Njuguna, J. (2016), “Lightweight composite structures in transport: Design, manufacturing, analysis and performance”, Lightweight Composite Structures in Transport: Design, Manufacturing, Analysis and Performance, pp. 1-453, doi: 10.1016/C2014-0-02646-9.

Olsson, R. (2012), “Modelling of impact damage zones in composite laminates for strength after impact”, The Aeronautical Journal, Vol. 116 No. 1186, pp. 1349-1365, doi: 10.1017/S0001924000007673.

Opelt, C.V., Cândido, G.M. and Rezende, M.C. (2018), “Compressive failure of fiber reinforced polymer composites – a fractographic study of the compression failure modes”, Materials Today Communications, Vol. 15, pp. 218-227, doi: 10.1016/J.MTCOMM.2018.03.012.

Peng, Y. et al. (2019), “Synergistic reinforcement of polyamide-based composites by combination of short and continuous carbon fibers via fused filament fabrication”, Composite Structures, Vol. 207, pp. 232-239, doi: 10.1016/J. COMPSTRUCT.2018.09.014.

Sadasivuni, K.K., Deshmukh, K. and Al-Maadeed, M.A.-A. (2020), 3D and 4D Printing of Polymer Nanocomposite Materials: Processes, Applications, and Challenges, Elsevier, Amsterdam.

Shonaike, G.O. (1988), “The effect of temperature on coldrolled nylon-6”, European Polymer Journal, Vol. 24 No. 11, pp. 1107-1110, doi: 10.1016/0014-3057(88)90072-9.

Swolfs, Y. and Pinho, A.S. (2016), “Designing and 3Dprinting continuous Fibre-Reinforced composites with a high fracture toughness”.

Tan, W. et al. (2015), “Predicting low velocity impact damage and Compression-After-Impact (CAI) behaviour of composite laminates”, Composites Part A: Applied Science and Manufacturing, Vol. 71, pp. 212-226, doi: 10.1016/J. COMPOSITESA.2015.01.025.

Taormina, G. et al. (2018), “3D printing processes for photocurable polymeric materials: technologies, materials, and future trends”, Journal of Applied Biomaterials & Functional Materials, Vol. 16 No. 3, pp. 151-160, doi: 10.1177/2280800018764770.

Zhang, D. et al. (2013), “A comparative study on low-velocity impact response of fabric composite laminates”, Materials & Design, Vol. 50, pp. 750-756, doi: 10.1016/J.MATDES. 2013.03.044.

Further reading

Composite materials handbook (2002), “3 polymer matrix composites: materials usage, design, and analysis”, Vol. 3, Composite Materials Handbook, AMSC.

Hechtel, K. and Author, D. (2022), “design considerations for the use of plastic materials in cryogenic environments click, learn more”.

Standard Test Method for Measuring the Damage Resistance of a Fiber-Reinforced Polymer Matrix Composite to a Drop-Weight Impact Event (2022), available at: www.astm.org/d7136_d7136m-12.html (accessed 4 February 2022).